Forty-Eighth Annual Allerton Conference
Allerton House, UIUC, Illinois, USA
September 29 - October 1, 2010

Electromagnetic Imaging Using Compressive Sensing

Marija M. Nikolić, Gongguo Tang, Antonije Djordjević, Arye Nehorai, *Fellow, IEEE,*

***Abstract*—We develop a near-field compressive sensing (CS) estimation scheme for localizing scattering objects in vacuum. The potential of CS for localizing sparse targets was demonstrated in previous work. We extend the standard far-field approach to near-field scenarios by employing the electric field integral equation to capture the mutual interference among targets. We show that the advanced modeling improves the capability to resolve closely spaced targets. We compare the performance of our algorithm with the performances of CS applied to point targets and beamforming. In this paper, we consider two-dimensional (2D) scatterers. However, the results and conclusions can be extended to three-dimensional (3D) problems.**

***Index Terms*—compressive sensing, sparse signal processing, radar, inverse scattering**

I. Introduction

We investigate the application of compressive sensing (CS) for solving inverse electromagnetic problems such as localizing targets placed in vacuum. This is typically an ill-posed problem unless some prior knowledge about the targets is available. Here, we exploit the sparseness of the targets.

The superior performance of sparse signal processing for estimating point targets in vacuum, with respect to standard techniques such as beamforming, was shown in [1]. The application of CS was further extended to subsurface imaging using ground penetrating radar measurements (GPR) [2] and through-the-wall imaging [3]. The analysis of the scattered signals using CS measurements was covered in [4]. The super-resolution properties of CS and time-reversal are closely related, as demonstrated in [5].

CS reconstruction aims at recovering a sparse signal from linear measurements of a usually underdetermined system. More precisely, suppose we have a k-sparse signal $\boldsymbol{x} \in \mathbb{F}^n$, that is, $\boldsymbol{x}$ has at most k non-zero components. We observe $\boldsymbol{y} \in \mathbb{F}^m$ through the following linear system:

$$\boldsymbol{y} = A\boldsymbol{x} + \boldsymbol{w}, \tag{1}$$

where $A \in \mathbb{F}^{m\times n}$ is the measurement/sensing matrix and $\boldsymbol{w} \in \mathbb{F}^m$ is the noise vector. Here the underlying field $\mathbb{F} = \mathbb{R}$ or $\mathbb{C}$. The measurement system is underdetermined because $m \ll n$ in general. This measurement model gained popularity in recent years due to the growing interest in CS [6], [7], a new framework for compression, sensing, and sampling that promises to break the sampling limit set by Shannon and Nyquist. Consider the noise-free case. Ideally, we wish to exploit the sparsity of $\boldsymbol{x}$ and reconstruct $\boldsymbol{x}$ through solving the following, unfortunately, NP-hard optimization problem:

$$\min \|\boldsymbol{x}\|_0 \ \text{ subject to } \ \boldsymbol{y} = A\boldsymbol{x}. \tag{2}$$

A major advance in sparse signal reconstruction is that we can actually replace the ℓ_0 norm with the convex ℓ_1 norm and can still recover $\boldsymbol{x}$ under certain conditions. This convex relaxation technique is employed in several very successful algorithms for sparse signal reconstruction, *e.g.,* basis pursuit [8], Dantzig selector [9], and LASSO estimator [10]. These algorithms can be applied to the noisy case as well.

We use the electric field integral equation to derive the estimation scheme. The emphasis is on the estimation of closely spaced objects. In contrast to the standard point target/far-field approximation ([1]), we use precise electromagnetic models to capture the mutual interference among targets. We show that the advanced modeling improves the capability of the algorithm to resolve targets. In this paper, we consider two-dimensional (2D) scatterers. However, the results and conclusions can be extended to three-dimensional (3D) problems.

II. 2D Measurement Model

We consider a 2D electromagnetic problem consisting of scatterers (targets) placed in vacuum and an array of sensors, as shown in Fig. 1. The goal is to estimate the locations of targets, which may be closely spaced, using CS and near-field array measurements. In previous studies (e.g., [1]), targets were treated as point or line scatterers in 3D or 2D, respectively. Assuming targets are in far-field, the observed signals are modeled as attenuated and delayed replicas of the transmitted signals. Instead, we derive a more general measurement model using the electric field integral equation (EFIE) [11]. The rationale is that more detailed electromagnetic modeling captures more information such as the mutual interference among targets, and consequently should result in more accurate estimation.

Suppose the sensors are infinitely long, thin line conductors, excited by an impressed axial electric field. In response to this excitation, equivalent surface currents are induced on the surfaces of all entities (sensors and targets). In this paper, we consider perfectly conducting scatterers. Hence, induced

G. Tang and A. Nehorai are with Department of Electrical and Systems Engineering, Washington University in St. Louis, St. Louis, MO 63130-1127; Email: nehorai@ese.wustl.edu.

M. M. Nikolić is with Department of Electrical and Systems Engineering, Washington University in St. Louis, St. Louis, MO and with School of Electrical Engineering, University of Belgrade, Serbia; Email: nikolic2@ese.wustl.edu.

A. Djordjević is with School of Electrical Engineering, University of Belgrade, Serbia.

This work was supported by the Department of Defense under the Air Force Office of Scientific Research MURI Grant FA9550-05-1-0443, ONR Grant N000140810849, and in part by Grant TR 11021 of the Serbian Ministry of Science and Technological Development.

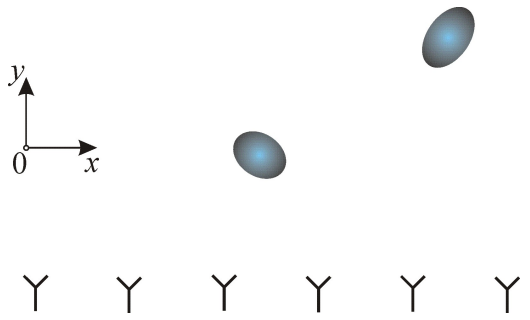

Fig. 1. Two scatterers and the sensing array (2D model).

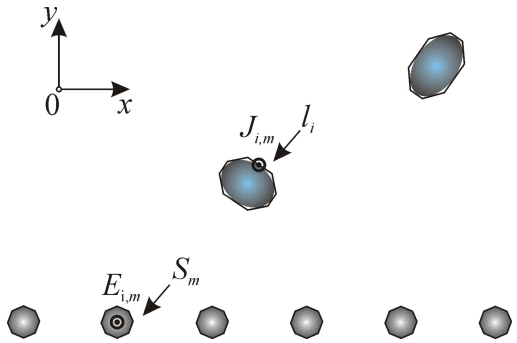

Fig. 2. Method of moments electromagnetic model for the forward problem in Fig. 1.

currents are electric, axial, and constant along the z axis. We wish to estimate those currents, since they uniquely determine the locations of the targets.

We approximate the induced current distribution with L equivalent current sources. We assume the current sources are uniformly distributed in the search space. Since the targets are sparse, most of the sources will have have zero currents. We aim at deriving a linear model

$$\boldsymbol{y} = G\boldsymbol{j} + \boldsymbol{w}, \tag{3}$$

where $\boldsymbol{j}$ is the vector with unknown currents, $\boldsymbol{y}$ is the measurement vector, G is the sensing matrix, and $\boldsymbol{w}$ is the noise vector. We use sparse signal reconstruction algorithms to retrieve the non-zero current coefficients, which correspond to the true target locations.

A. Electromagnetic Modeling: Forward Problem

We apply the point matching to the electric field integral equation [11], [12] to compute the measurement model (3). According to the boundary conditions, the tangential component of the electric field on the surfaces of all conductors is zero. In the transverse mode this condition reduces to

$$E = E_z = 0. \tag{4}$$

The electric field is expressed in terms of induced currents as

$$E(\boldsymbol{r}) = -\jmath\omega\mu_0 \int_S J(\boldsymbol{r}')g(r)ds + E_{\mathrm{i}}(\boldsymbol{r}), r = |\boldsymbol{r} - \boldsymbol{r}'|, \tag{5}$$

where J is the axial surface current, E_{i} is the impressed electric field, $\boldsymbol{r}$ is the field point location, $\boldsymbol{r}'$ is the source point location, g is Green's function, and S is the union of all boundary surfaces (circumferences of all entities). The exact Green's function for 2D case is

$$g(r) = -\frac{\jmath}{4} H_0^{(2)}(kr), \tag{6}$$

where $H_0^{(2)}$ is the Henkel function of the second kind and order zero, and $k = \omega\sqrt{\mu_0\epsilon_0}$ is the phase coefficient. We use the pulse expansion to approximate the current distribution [11], [12]. To this end we divide the circumferences of all entities into a number of line segments l_i, $i = 1, \ldots, N$, and assume the currents to be constant along each segment (Fig. 2).

After substituting the current approximation, (5) becomes

$$E(\boldsymbol{r}) = -\zeta \sum_{i=1}^{N} J_i \int_{l_i} H_0^{(2)}(kr)d(ks) + E_{\mathrm{i}}(\boldsymbol{r}), \tag{7}$$

where J_i is the current coefficient of the ith segment (l_i) and ζ is the wave impedance in vacuum. We apply the point matching method to compute the unknown current coefficients. When the mth sensor is excited, the system of equation reads

$$E(\boldsymbol{r}_j) = -\zeta \sum_{i=1}^{N} J_{i,m} \int_{l_i} H_0^{(2)}(kr)d(ks) + E_{\mathrm{i},m}(\boldsymbol{r}_j), \tag{8}$$

$$E_{\mathrm{i},m}(\boldsymbol{r}_j) = \begin{cases} 1 & \text{if } \boldsymbol{r}_j \in S_m, \\ 0 & \text{otherwise.} \end{cases} \tag{9}$$

where $\boldsymbol{r}_j$, for $j = 1, \ldots, N$, are the matching points located at the segment midpoints, and S_m is the boundary of the mth sensor. In matrix form this reads

$$G\boldsymbol{j}_m = \boldsymbol{e}_{\mathrm{i},m}, \tag{10}$$

where

$$G = \begin{bmatrix} G_{11} & \ldots & G_{1N} \\ \vdots & \ddots & \vdots \\ G_{N1} & \ldots & G_{NN} \end{bmatrix}, \tag{11}$$

$$G_{ij} = -\zeta \int_{l_i} H_0^{(2)}(kr)d(ks), r = |\boldsymbol{r}_j - \boldsymbol{r}'|, \tag{12}$$

$$\boldsymbol{j}_m = \begin{bmatrix} J_{1,m} & \ldots & J_{N,m} \end{bmatrix}^T, \tag{13}$$

$$\boldsymbol{e}_{\mathrm{i},m} = \begin{bmatrix} E_{\mathrm{i},m}(\boldsymbol{r}_1) & \ldots & E_{\mathrm{i},m}(\boldsymbol{r}_N) \end{bmatrix}^T. \tag{14}$$

B. Electromagnetic Modeling: Inverse Problem

If the targets are completely known, (10) represents a system of linear equations for the unknown current coefficients induced on the surfaces of all entities ($\boldsymbol{j}_m$) when the mth sensor is excited. In the inverse problem, we have no prior knowledge about the shape of the targets. Hence, the locations of the current elements are also unknown. In order to estimate the

induced currents, we divide the search space into a quadratic mesh. Each side of the square element in the mesh stands for a surface current source. The cross-sections of the currents sources are parallel to the x or the y axis as shown in Fig. 3. (The currents are oriented along the z axis.) An example of a current element is colored in red in Fig. 3. We suppose the scatterers are not electrically large, and therefore use constant current sources. Otherwise the current distribution of each source can be represented by using e.g., polynomials ([4]).

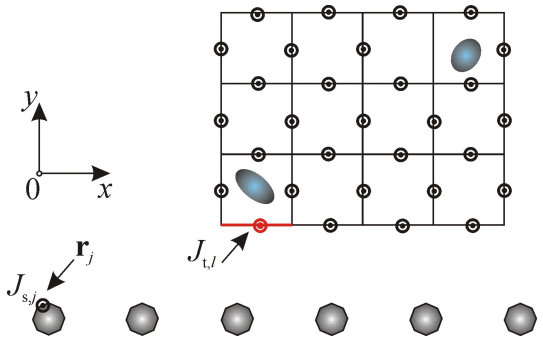

Fig. 3. Method of moments electromagnetic model for the inverse problem in Fig. 1.

We separate in (10) the induced currents, as well as the matching points, belonging to sensors and targets

$$\begin{bmatrix} G_{\rm ss} & G_{\rm st} \\ G_{\rm ts} & G_{\rm tt} \end{bmatrix} \begin{bmatrix} \boldsymbol{j}_{{\rm s},m} \\ \boldsymbol{j}_{{\rm t},m} \end{bmatrix} = \begin{bmatrix} \boldsymbol{e}_{{\rm i},m} \\ \boldsymbol{0} \end{bmatrix}, \tag{15}$$

$$\boldsymbol{j}_{{\rm s},m} = \begin{bmatrix} J_{1,m} & \dots & J_{N_{\rm s},m} \end{bmatrix}^T, \tag{16}$$

$$\boldsymbol{j}_{{\rm t},m} = \begin{bmatrix} J_{N_{\rm s}+1,m} & \dots & J_{N,m} \end{bmatrix}^T, \tag{17}$$

$$\boldsymbol{e}_{{\rm i},m} = \begin{bmatrix} E_{{\rm i},m}(\boldsymbol{r}_1) & \dots & E_{{\rm i},m}(\boldsymbol{r}_{N_{\rm s}}) \end{bmatrix}^T, \tag{18}$$

$\boldsymbol{j}_{{\rm s},m} \in \mathbb{C}^{N_{\rm s}}$ is the vector of current coefficients on sensors, $\boldsymbol{j}_{{\rm t},m} \in \mathbb{C}^{N_{\rm t}}$ is the vector of current coefficients on targets, $\boldsymbol{e}_{{\rm i},m} \in \mathbb{C}^{N_{\rm s}}$ is the excitation vector, and $G_{\rm ss} \in \mathbb{C}^{N_{\rm s}\times N_{\rm s}}$,$G_{\rm tt} \in \mathbb{C}^{N_{\rm t}\times N_{\rm t}}$, $G_{\rm st} = G_{\rm ts}^T \in \mathbb{C}^{N_{\rm s}\times N_{\rm t}}$ are the submatrices of the matrix G. In (15), $N_{\rm s}$ is the number of the current coefficients (matching points) on the sensors and $N_{\rm t}$ is the number of the current coefficients (matching points) on the targets. Sensors are thin line conductors centered at $\boldsymbol{r}_1, \dots \boldsymbol{r}_M$.

In the inverse problem, we use the matching points on the sensors only, hence (15) becomes

$$\begin{bmatrix} G_{\rm ss} & G_{\rm st} \end{bmatrix} \begin{bmatrix} \boldsymbol{j}_{{\rm s},m} \\ \boldsymbol{j}_{{\rm t},m} \end{bmatrix} = \boldsymbol{e}_{{\rm i},m} \tag{19}$$

or

$$G_{\rm st}\boldsymbol{j}_{{\rm t},m} = \boldsymbol{e}_{{\rm i},m} - G_{\rm ss}\boldsymbol{j}_{{\rm s},m}. \tag{20}$$

If there are no targets, the complete set of equations reads

$$G_{\rm ss}\boldsymbol{j}^0_{{\rm s},m} = \boldsymbol{e}_{{\rm i},m}, \tag{21}$$

where $\boldsymbol{j}^0_{{\rm s},m}$ is the vector of induced currents in the isolated array. We subtract (21) from (20) to obtain the measurement model

$$G_{\rm st}\boldsymbol{j}_{{\rm t},m} = \underbrace{G_{\rm ss}(\boldsymbol{j}^0_{{\rm s},m} - \boldsymbol{j}_{{\rm s},m})}_{\boldsymbol{y}_m}, \tag{22}$$

where $\boldsymbol{y}_m$ is the measurement vector. (The observed values are the currents in the sensors and therefore $\boldsymbol{y}_m$ is completely known.) We adopt: $N_{\rm s} = M$ and $N_{\rm t} = L$, where L is the number of constant current sources in the mesh. We assume that the measurements are corrupted with additive white Gaussian noise. Therefore, the measurement equation, when the mth sensor is excited, reads

$$\boldsymbol{y}_m = G_{\rm st}\boldsymbol{j}_{{\rm t},m} + \boldsymbol{w}_m, \tag{23}$$

where $w_m \in \mathbb{C}^L$ is the noise vector. In the remainder of the paper we simplify the notation as $G_{\rm st} \equiv G$ and $\boldsymbol{j}_{{\rm t},m} \equiv \boldsymbol{j}_m$.

The current vector $\boldsymbol{j}_m$ is sparse and complex. To recover the current sources, we solve the following optimization problem

$$\hat{\boldsymbol{j}}_m = \arg\min_{\boldsymbol{j}_m} \|\boldsymbol{y}_m - G\boldsymbol{j}_m\|_2 + \lambda\|\boldsymbol{j}_m\|_1, \tag{24}$$

using the CVX [13], a package for specifying and solving convex programs [14]. We compute the image by assigning the absolute value of the current to a corresponding pixel, i.e.,

$$P_m = |\hat{\boldsymbol{j}}_m|, \tag{25}$$

where P_m is the image computed when the mth sensor is excited. If all sensors in the array work as transmitters and receivers, the joint image is

$$P = \sum_{m=1}^{M} P_m. \tag{26}$$

We perform the estimation at different frequencies separately since the current distribution may vary significantly with frequency. The combined solution is

$$P = \sum_{i=1}^{I} P(f_i), \tag{27}$$

where $P(f_i)$ is the solution at the ith frequency, $i = 1, \dots, I$.

III. Example

We study the resolution of the electromagnetic imaging algorithm described in Section II. We consider two metallic scatterers with circular cross-sections and diameters $D = 3\,{\rm cm}$. We assume the measurements are taken by a uniform linear array at the discrete set of frequencies: $f \in [0.9\,{\rm GHz}, 1\,{\rm GHz}, 1.1\,{\rm GHz}]$. The array consists of 10 sensors and it is parallel to x-axis. The first element of the array is located at $(-2\,{\rm m}, 0)$, and the separation between adjacent sensors is $0.4\,{\rm m}$. We adopt ${\rm SNR} = 20\,{\rm dB}$. In the first example, the centers of the targets are at $(0{\rm m}, 2\,{\rm m})$ and $(0.15\,{\rm m}, 2\,{\rm m})$. The distance between the targets is $15\,{\rm cm}$, which is approximately the Rayleigh resolution for the given array aperture and stand-off distance.

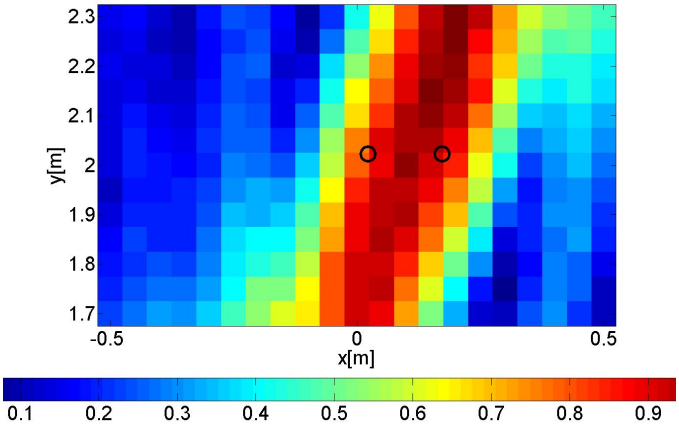

Fig. 4. Electromagnetic imaging using beamforming. Separation between targets is $0.15\mathrm{m}$.

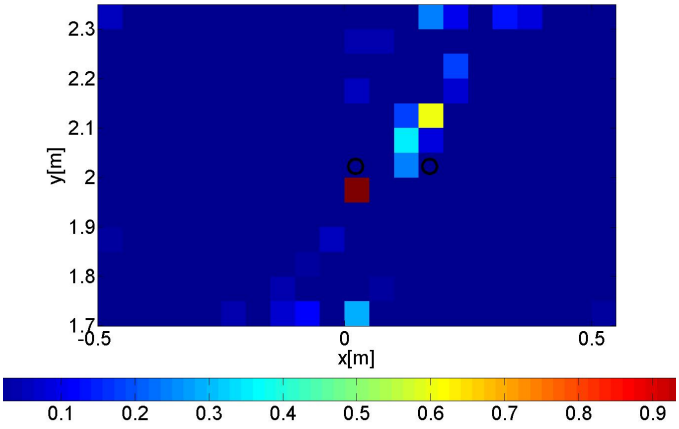

Fig. 5. Electromagnetic imaging using near-field CS. Separation between targets is $0.15\mathrm{m}$.

We assume that only one sensor in the array transmits signals, while others are the receivers. In the numerical experiment, we adopt that the rightmost sensor is the transmitter $(-2\,\mathrm{m}, 0)$. We first compute rough estimates of the target locations using beamforming

$$P(\boldsymbol{r}_l) = \sum_{i=1}^{I} |P(\boldsymbol{r}_l; f_i)| \tag{28}$$

with

$$P(\boldsymbol{r}_l; f_i) = \sum_{m,n} (j_{m,n} - j^0_{m,n}) \exp(\jmath 2\pi f_i \tau^l_{mn}) \tag{29}$$

and

$$\tau^l_{mn} = (|\boldsymbol{r}_m - \boldsymbol{r}_l| + |\boldsymbol{r}_n - r_l|)/c_0, \tag{30}$$

where $P(\boldsymbol{r}_l)$ is the value of the lth pixel, $j_{m,n}$ is the current in the nth sensor when the mth sensor is excited, and $j^0_{m,n}$ is the current in the nth sensor when the mth sensor is excited and the array is isolated. The result is shown in Fig. 4.

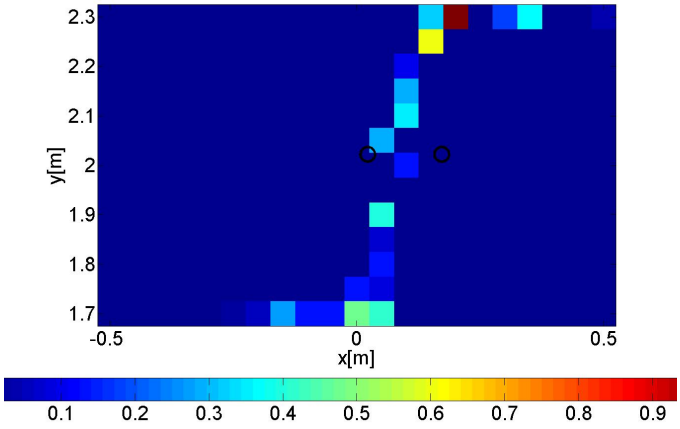

Fig. 6. Electromagnetic imaging using far-field CS. Separation between targets is $0.15\mathrm{m}$.

The image resolution is poor, and the target traces are not separable. We now compute the image using the near-field CS. We divide the search space into a mesh: $\Delta_x = \Delta_y = 0.05\,\mathrm{m}$ and set $\lambda = 1$. The obtained image is shown in Fig. 5. In contrast to the image obtained by beamforming, there are two distinct pixels corresponding to targets locations. The y coordinate of the first target is offset for $5\,\mathrm{cm}$ and the second for $10\,\mathrm{cm}$. We also compute the image using the standard far-field approximation [1]. The computed image is shown in Fig. 6. The target space is small due to the sparsity constraint, but the algorithm failed to estimate the locations of the targets, as well as their number. The increased resolution in the case of near-field measurements is also noticed in [15] for the images computed using diffraction tomography (DT).

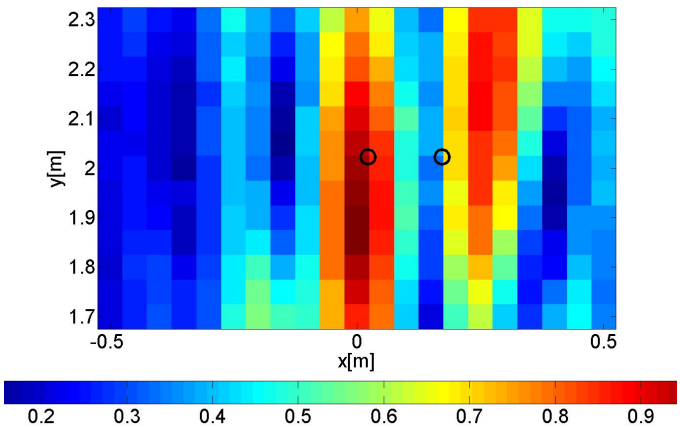

Fig. 7. Electromagnetic imaging using beamforming. Separation between targets is $0.2\mathrm{m}$.

We repeat the experiment with targets' separation of $0.2\,\mathrm{m}$. The results obtained by beamforming, CS near-field formulation, and CS far-field formulation are shown in Fig. 7, Fig. 8, and Fig. 9, respectively. When the separation is beyond the

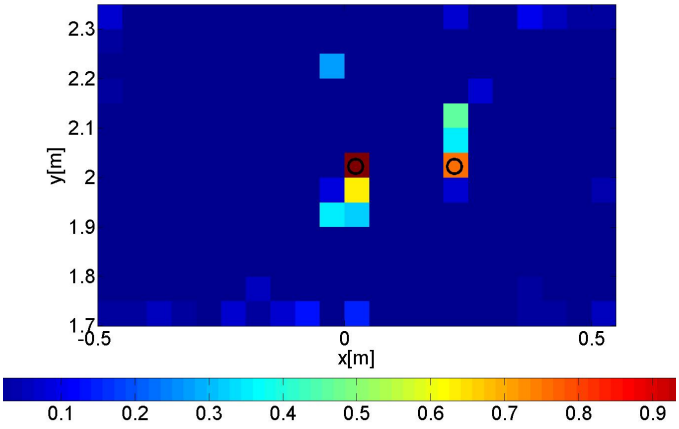

Fig. 8. Electromagnetic imaging using near-field CS. Separation between targets is 0.2m.

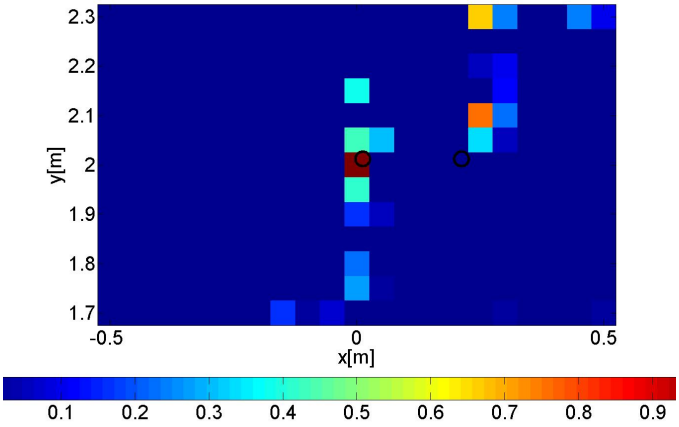

Fig. 9. Electromagnetic imaging using far-field CS. Separation between targets is 0.2m.

Rayleigh limit, the targets are resolved irrespectively of the method. However, the most accurate estimate is obtained using the CS near-field estimation model, at the expense of the largest computational burden.

IV. Conclusion

We developed a near-field estimation framework for localizing sparse targets in vacuum. We demonstrated that refined electromagnetic modeling based on the electric field integral equation produces high-resolution images. We showed that the capability of the algorithm to resolve closely spaced targets is better than that of standard far-field approach and beamforming. The improved performance is achieved at the cost of higher computational complexity.

References

[1] D. M. Malioutov, M. Cetin, and A. S. Willsky, "Sparse signal reconstruction perspective for source localization with sensor arrays," *IEEE Trans. on Signal Processing*, vol. 53, no. 8, pp. 3010–3022, 2005.

[2] A. C. Gurbuz, J. H. McClellan, W. R. Scott, "A compressive sensing data acquisition and imaging method for stepped frequency GPRs," *IEEE Trans. on Signal Processing*, vol. 57, no. 7, pp. 2640–2650, July 2009.

[3] Q. Huang, L. Qu, B. Wu, G. Fang, "UWB through-wall imaging based on compressive sensing," *IEEE Trans. Geosci. Remote Sens.*, vol. 48, no. 3, pp. 1408–1415, Mar. 2010.

[4] L. Carin, D. Liu, W. Lin, B. Guo "Compressive sensing for multi-static scattering analysis," *Journal of Computational Physics*, vol. 228, no. 9, pp. 3464–3477, May 2009.

[5] L. Carin, "On the relationship between compressive sensing and random sensor arrays," *IEEE Antennas Propag. Mag.*, vol. 5', no. 5, pp. 72–81, Oct. 2009.

[6] E. J. Candès and M. B. Wakin, "An introduction to compressive sampling," *IEEE Signal Process. Mag.*, vol. 25, no. 2, pp. 21–30, Mar. 2008.

[7] R. G. Baraniuk, "Compressive sensing [lecture notes]," *IEEE Signal Process. Mag.*, vol. 24, no. 4, pp. 118–121, July 2007.

[8] S. Chen, D. L. Donoho, and M. A. Saunders, "Atomic decomposition by basis pursuit," *SIAM J. Sci. Comp.*, vol. 20, no. 1, pp. 33–61, 1998.

[9] E. J. Candès and T. Tao, "The Dantzig selector: Statistical estimation when p is much larger than n," *Ann. Statist.*, vol. 35, pp. 2313–2351, 2007.

[10] R. Tibshirani, "Regression shrinkage and selection via lasso," *J. Roy. Statist. Soc. Ser. B*, vol. 58, pp. 267–288.

[11] R. F. Harrington, *Field Computation by Moment Methods*, Malabar, FL, 1982.

[12] A. R. Djordjevic, T. K. Sarkar, S. M. Rao " Analysis of finite conductivity cylindrical conductors excited by axially-independent TM electromagnetic field," *IEEE Microwave Theory Techn.* , vol. 33, no. 10, pp. 960–966, Oct. 1985.

[13] M. Grant and S. Boyd, CVX: *Matlab software for disciplined convex programming*, http://stanford.edu/ boyd/cvx, June 2009.

[14] M. Grant and S. Boyd. *Graph implementations for nonsmooth convex programs*, Recent Advances in Learning and Control (a tribute to M. Vidyasagar), V. Blondel, S. Boyd, and H. Kimura, editors, pages 95-110, Lecture Notes in Control and Information Sciences, Springer, 2008.

[15] T.J. Cui, W.C. Chew, X.X. Yin, and W. Hong, "Study of Resolution and Super Resolution in Electromagnetic Imaging for Half-Space Problems," *IEEE Trans. Antennas Propagat*, vol. 52, no. 6, pp. 1298–1411, Jun. 2004.

[16] B. Kolundzija et al., WIPL-D Pro v6.1: 3D Electromagnetic Solver, Professional Edition. User's Manual, WIPL-D d.o.o., 2006.